Nuclear Instruments and Methods in Physics Research B 557 (2024) 165533

Contents lists available at ScienceDirect

Nuclear Inst. and Methods in Physics Research, B

journal homepage: www.elsevier.com/locate/nimb

Full Length Article

The effect of ion implantation and annealing temperatures on the migration behavior of ruthenium in glassy carbon

T.A.O. Jafer [a,*], O.S. Odutemowo [a], H.A.A. Abdelbagi [a,b], T.T. Thabethe [a], J.B. Malherbe [a]

[a] Physics Department, University of Pretoria, Pretoria, South Africa
[b] PhysicsDepartment, University of Zululand, KwaDlangezwa, 3886, South Africa

ARTICLE INFO

Keywords:
Ruthenium
Glassy carbon
Aggregation
Defects
Surface roughness

ABSTRACT

Nuclear waste storage materials are inevitable in nuclear industry for preventing the release of radioactive waste products. Glassy carbon has been considered being beneficial to be used in the dry cask needed for nuclear waste storage. Thus, we studied the migration of ruthenium implanted in glassy carbon upon annealing. Our investigations show that ruthenium implantation caused defects in the glassy carbon structure, with more defects observed in the room temperature as-implanted samples compared to those implanted at 200 °C. Annealing the as-implanted samples from 500 to 800 °C showed no significant change in the ruthenium depth profiles, indicating the non-diffusivity of ruthenium in glassy carbon at these temperatures. However, annealing at higher temperatures (from 900 and 1300 °C) resulted in an increase in the maximum depth profile peaks, accompanied by a shift towards the surface, and a decrease in the full-width at half-maximum. These changes indicate the aggregation of ruthenium atoms in the near-surface region. Additionally, more ruthenium aggregation was observed in room temperature implanted samples compared to those implanted at 200 °C. This difference is attributed to the higher concentration of defects in room temperature implanted samples, which promotes ruthenium aggregation. Moreover, the migration and aggregation of ruthenium in the near-surface region contributed to an increase in the surface roughness of the glassy carbon.

1. Introduction

Addressing the global challenge of sustainable energy production with minimal carbon emissions is paramount. The conventional use of fossil fuels for energy generation significantly contributes to carbon dioxide emissions, exacerbating climate change. In contrast, nuclear energy stands out as one of the cleanest energy sources, boasting minimal carbon footprint [1]. However, the utilization of nuclear power leads to the generation of substantial nuclear waste, necessitating meticulous management to prevent environmental and health risks. For instance, a nuclear reactor operating with 1 GW produces approximately 20,000 – 27,000 kg of spent nuclear fuel (SNF) annually [2]. Proper waste management is imperative to mitigate the hazards posed by radioactive waste leakage during transportation, storage, or unforeseen incidents [3]. Therefore, nuclear waste management remains a persistent concern for the industry, leading many countries to hesitate in embracing nuclear energy [4].

Developing robust nuclear waste containers is a critical aspect of waste management. These containers must ensure the long-term stability of radioactive materials, isolate radioactivity during transportation, storage, and disposal, and prevent leakage. While traditional containers are usually made of metals like stainless steel, iron, copper, nickel-based alloys, and titanium alloys [5], these materials are prone to degradation over time, which may result in radioactive material leaking into the environment. Hence, there is a growing need for storage containers with a longer lifespan. This can be achieved by improving the material from which the containers are made. Glassy carbon, a synthetic form of carbon that exhibits glassy, ceramic, and graphite properties, has emerged as a potential material for nuclear waste storage containers. Its unique characteristics, such asresistance to high temperature and corrosion, low density, biocompatibility, and impermeability to liquids and gases, along with its ability to trap some radioactive elements, contribute to its suitability for this purpose [6–8]. These outstanding properties position glassy carbon as a promising candidate, offering enhanced durability and containment capabilities compared to conventional options.

Moreover, glassy carbon must meet specific criteria to serve as a material for containing nuclear waste [3,9]. These requirements include

* Corresponding author.
E-mail address: Tasabeeh.Jafer@gmail.com (T.A.O. Jafer).

https://doi.org/10.1016/j.nimb.2024.165533
Received 20 May 2024; Received in revised form 25 August 2024; Accepted 14 September 2024
Available online 18 September 2024

high resistance to radiation damage from nuclear waste and inhibiting the diffusion of radioactive fission elements commonly found in nuclear waste containers (e.g., ruthenium). The suitability of glassy carbon as a diffusion barrier against various radioactive fission products (such as Cs, Sr, Cd, In, Ag, Se, Xe) has been thoroughly investigated [7–17]. These studies revealed that the implantation of fission products into glassy carbon leads to some changes in its structure (e.g., implantation at room temperature leads to amorphization, whereas implantation at higher temperatures results in fewer structural defects). However, recrystallization of amorphous glassy carbon (i.e., in samples implanted at room temperature) was observed after annealing [7–11,13]. Furthermore, after annealing at different temperatures, different impurities implanted in glassy carbon (such as Sr, Eu, Se and Xe) showed different migration behaviors (such as Fickian diffusion and segregation). Overall, previous studies suggest a correlation between the structure of glassy carbon and the migration behavior of implanted fission products [7–17].

In our previous study, ruthenium ions were implanted into glassy carbon at room temperature, and then the as-implanted samples were sequentially annealed from 1000 to 1300 °C [18]. We observed that ruthenium tended to aggregate within the implanted region of the glassy carbon starting from the initial annealing stage (i.e., 1000 °C). However, the behavior of ruthenium atoms in glassy carbon at lower annealing temperatures remains unexplored and requires further investigation. Additionally, the heat generated by the radioactivity of nuclear waste can elevate temperatures within the nuclear waste storage system [2]. To simulate the radiation conditions expected within the nuclear waste storage material, the glassy carbon material was implanted with ruthenium (in this study) at both room temperature and a high temperature of 200 °C, each to a fluence of 1×10^{16} ions/cm^2. This approach aimed to compare the radiation-induced damage in the glassy carbon substrates resulting from ruthenium implantation at varying temperatures. Furthermore, this study investigates the annealing of radiation damage and the migration behavior of ruthenium within the glassy carbon substrate after annealing at low and high temperatures.

2. Experimental Method

SIGRADUR®G glassy carbon samples from Hochtemperature-Werkstoffe GmbH, Germany were used in this study. The as-received samples were implanted with 150 keV ruthenium (Ru) ions to a fluence of 1×10^{16} ions/cm^2 in vacuum at room temperature and 200 °C. The as-implanted samples were annealed sequentially (in vacuum) at low and high temperatures ranging from 500 to 1000 °C and from 1000 to 1300 °C, respectively, in steps of 100 °C and for 5 h. A computer-controlled Webb 77 graphite furnace was used for the annealing process. The structural changes and surface modification in the glassy carbon substrates due to implantation and annealing were investigated by Raman spectroscopy, X-ray diffraction (XRD) and atomic force microscopy (AFM). Moreover, Rutherford backscattering spectrometry (RBS) was used to study the migration behavior of ruthenium atoms in glassy carbon upon annealing.

WITec alpha 300 confocal Raman spectroscopy instrument was used to monitor the influence of ruthenium implantation and annealing on the microstructure of glassy carbon substrate. Using a 100 × 0.9NA objective lens, the Raman spectra were acquired at 532 nm with 5mW laser excitation. The penetration depth of the 532 nm laser in glassy carbon was calculated by dividing the wavelength by the extinction coefficient, as shown in the following equation, $z = \lambda/4\pi k$ [19], and found to be 59 nm. The Raman spectra of glassy carbon were analyzed by first correcting the baseline of the spectral lines using a linear background correction. Subsequently, using OriginLab software program [20], the spectra were fitted using both Gaussian and Breit-Wigner-Fano (BWF) functions to determine the full width at half maximum (FWHM) and peaks positions.

Grazing incidence X-ray diffraction (GIXRD) analysis was used to study the structural changes and determine the strains in the glassy carbon after implantation and annealing. A Bruker D8 Discover XRD system with a Cu Kα radiation source (1.54184 Å) was used to acquire the GIXRD spectra of the glassy carbon samples. The incident angle was 4° and the 2θ step size was 0.04°. The penetration depth of X-rays in glassy carbon was calculated in our previous study and found to be 3 μm [18].

Atomic force microscopy (AFM) was used to study the surface topography of the virgin glassy carbon surfaces after implantation and annealing processes. The Dimension Icon AFM system was used to obtain AFM images. The system operates in contact mode and has a sharp nitride lever (SNL) probe with a tip radius of 2 nm, a spring constant of 0.30 N/m and a scan rate of 0.3 Hz. The resonance frequency of the SNL probe was between 40 and 75 kHz. AFM images obtained during the analysis of all samples were further analyzed using Nano-Scope Analysis (Bruker, USA), to determine the surface roughness [21,22].

Rutherford backscattering spectrometry (RBS) was used to monitor the migration behavior and depth profiles of ruthenium in glassy carbon samples before and after annealing. Helium ions with an energy of 1.6 MeV were used in the RBS measurements. The beam spot size was about 1 mm and the depth resolution was about 3 nm. The backscattered He ions were detected using a silicon surface barrier detector set at a 165° and a charge of 8 μC was collected per measurement. The measurement was repeated three times for each sample to reduce noise in the RBS spectra. Throughout the study, the maximum beam current was kept at15 nA to ensure uniformity.

3. Results and discussion

3.1. TRIM simulations

Fig. 1 shows the comparison between the RBS depth profile of Ru and the theoretical depth profile obtained by TRIM ion distribution simulation software [23]. These simulations were conducted using a substrate density of 1.42 g/cm^3, representing the density of the virgin Sigradur®G glassy carbon samples used in this study. Furthermore, TRIM simulations were also used to determine the displacement per atom (dpa) introduced by Ru implantation into glassy carbon.

According to our experimental results, Ru implanted at room temperature and 200 °C exhibit depth profiles with R_p values of 116.5 ± 3 and 116 ± 3 nm, respectively. These values are comparable with the 115 nm of the TRIM results. However, the difference between the range straggling, ΔR_p, obtained from RBS (31.2 ± 3 nm) and TRIM (24.4 nm) is

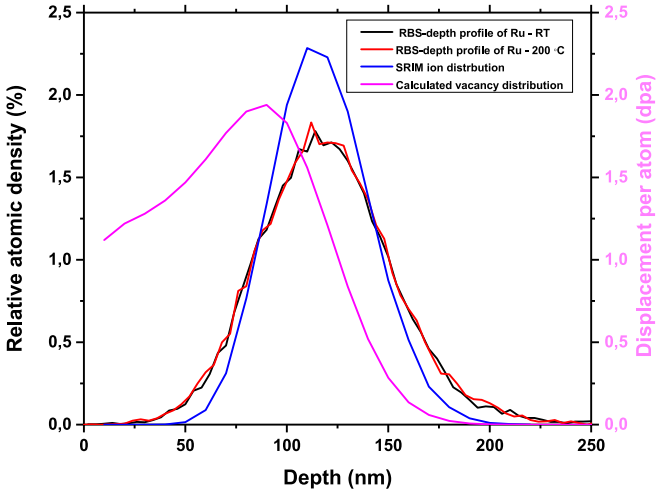

Fig. 1. RBS depth profiles of Ru ions implanted in glassy carbon at room temperature and 200 °C compared with TRIM simulation profile. The damage in dpa is also shown (in magenta) using the ions fluence of 1×10^{16}cm^{-2}.

about 24.5 %, which exceeds TRIM accuracy (i.e., 5–10 %). This discrepancy in the ΔR_P could be as a result of the trapping of some of the implanted ions in the pores contained within the glassy carbon structure [24]. This trapping of the ions causes the ΔR_P to be higher than expected. This phenomenon could be further investigated to gain a better understanding of the trapping and its effects. Furthermore, the discrepancy in the ΔR_P could also be due to the surface roughness of the as-implanted samples (which is equal to 0.4 nm – see AFM results) which can lead to a broader ion distribution than suggested by TRIM (TRIM considers the target as amorphous and having a smooth surface).

As shown in Fig. 1, the maximum damage level is 1.9 dpa obtained from TRIM simulations. This is significantly higher than the critical displacement per atom (dpa) value of 0.2 dpa required to amorphize glassy carbon [25]. Thus, the simulation of Ru in the glassy carbon (at the ion fluence of 1×10^{16} cm^{-2}) implies an amorphization thickness of about 155 nm in the glassy carbon substrate – see Fig. 1. This result is in good agreement with the Raman results shown in Fig. 2 below.

3.2. Raman results

Fig. 2 compares the Raman spectrum of virgin glassy carbon with that of implanted glassy carbon with Ru. Raman spectrum of virgin glassy carbon sample shows the D and G characteristic bands at positions 1346 cm^{-1} and 1587 cm^{-1}, respectively. The D and G peaks originate from the disordered sp^3 bonds and sp^2 vibrations of graphite, respectively [26]. These two peaks of the glassy carbon indicate the presence of small graphitic crystallites imbedded in the amorphous matrix [8]. The D and G peaks merged into a single broadband after implantation at room temperature and 200 °C. Only amorphous carbon structures have Raman spectra similar to those obtained from the as-implanted glassy carbon [25,27–30]. This indicates the amorphization of the graphitic crystallites in the implanted glassy carbon samples [8,26]. However, a broader peak was present in the Raman spectrum of the as-implanted samples at 200 °C compared to those implanted at room temperature – see Fig. 2. Adeojo *et al.* [17] and McCulloch *et al.* [30] also presented similar results, concluding that the magnitude of radiation damage in the room temperature implanted sample is greater than that in the 200 °C implanted sample.

Raman spectra of virgin glassy carbon samples, as-implanted at room temperature and 200 °C, and annealed samples at temperatures from 500 to 1000 °C are shown in Fig. 3. Initial annealing at 500 °C showed broad D and G peaks, indicating partial recrystallization of glassy carbon

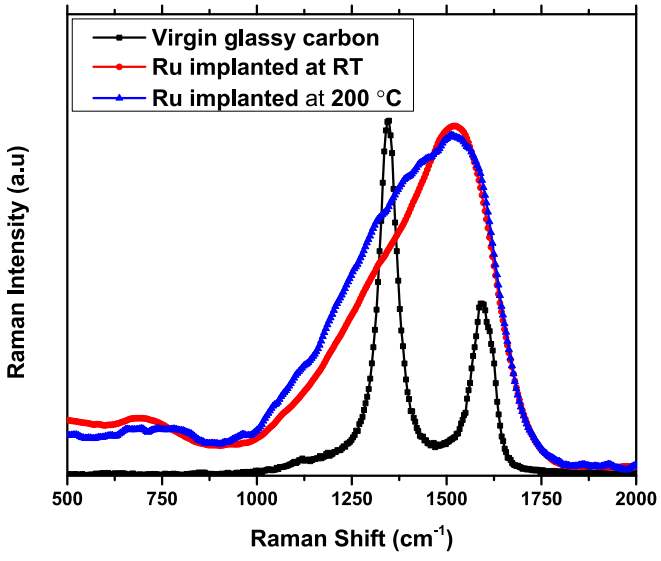

Fig. 2. Raman spectra of glassy carbon before and after ruthenium implantation at room temperature and 200 °C.

after annealing. The observed intensity of the re-grown G peak is higher than that of the D peak. This was more apparent in the implanted samples at room temperature – see Fig. 3. However, further annealing from 600 °C to 1000 °C resulted in the enhancement of the D peak intensity and a reduction in the G peak width. This indicates that some recovery of the glassy carbon structure increased with the increasing annealing temperature [7,10–11,16–17,24]. Moreover, at 1000 °C, the intensity of the D and G peak appears to be the same. It is noteworthy that this is in contrast to the Raman spectrum obtained for virgin glassy carbon, which shows a more distinct D peak. This is further proof that annealing at 1000 °C did not completely remove all the damage (in glassy carbon) introduced by Ru ion implantation.

Fig. 4 shows Raman spectra of Ru implanted glassy carbon at room temperature and 200 °C and annealed at higher temperatures, i.e., sequentially from 1000 to 1300 °C. As-implanted glassy carbon samples that were annealed at temperatures ranging from 1000 to 1300 °C showed re-growth of the Raman D and G peaks. Similar to samples annealed at lower temperatures, this indicates the recrystallization of glassy carbon. However, the structure did not fully return to its original state of virgin glassy carbon even after annealing at 1300 °C. This is further proof that annealing of as-implanted samples within the temperature ranges investigated in this study did not completely remove all radiation damage in the glassy carbon.

Fig. 5 shows the FWHMs of the G peaks of the acquired spectra before and after annealing of the glassy carbon samples implanted with Ru at room temperature and 200 °C. From Fig. 5, the FWHM value of the G peak increased from 31 ± 2 cm^{-1} (virgin glassy carbon) to 155 ± 2 cm^{-1} and 136 ± 2 cm^{-1} after implantation with Ru at room temperature and 200 °C, respectively. This broadening is due to the introduction of disorder (point defects) within the glassy carbon structure [8,13,26,31]. However, the G peak in room temperature implanted samples is broader than that in 200 °C implanted samples. This indicates that samples implanted at room temperature have more defects than those implanted at 200 °C [17]. Annealing from 500 to 1000 °C and from 1000 to 1300 °C resulted in a decrease in FWHM in all samples. The decrease in FWHM was an indication of the removal of some defects (annealing of radiation damage introduced by Ru ion implantation) [8,13,18]. However, annealing caused more decreases in the FWHMs for samples implanted at 200 °C compared to samples implanted at room temperature and annealed under the same conditions. This indicates that samples implanted at 200 °C have less defects than samples implanted at RT, all annealed from 500 to 1300 °C. This could be due to the initial number of defects in glassy carbon introduced by the ion implantation process (where implantation at room temperature caused more radiation damage/defects than those implanted at 200 °C). Moreover, at 1300 °C, FWHM values are 45 ± 2 and 40 ± 2 cm^{-1} for room temperature and 200 °C implanted samples, respectively. These values are higher than 31 ± 2 cm^{-1} for virgin glassy carbon. This also indicates that annealing did not completely remove all the damage introduced by the Ru ion implantation [3].

Comparing Fig. 5 (a) with (b), it is clear that annealing at 1000 °C exhibit a wider FWHM than those samples annealed sequentially up to 1000 °C. This indicates that samples annealed at 1000 °C have more defects than samples annealed sequentially up to 1000 °C, where sequential annealing from 500 to 900 °C caused partial removal of the defects. Ru migration in glassy carbon is influenced by defects in these samples, as will be discussed later in this study.

Fig. 6 shows the positions of the G peaks of the acquired spectra before and after annealing of the glassy carbon samples implanted with Ru at room temperature and 200 °C. The G peak of virgin glassy carbon is located at 0 °C. After Ru ion implantation, the G peak position shifted to a lower wavenumber. The shift of the Raman peak to a higher or lower wavenumber can be attributed to stress [32]. The type of residual stress associated with the Raman peak shift to a lower wavenumber (compared to the G peak of virgin glassy carbon) is tensile stress [32]. Which means the as-implanted samples were under tensile stress due to ion

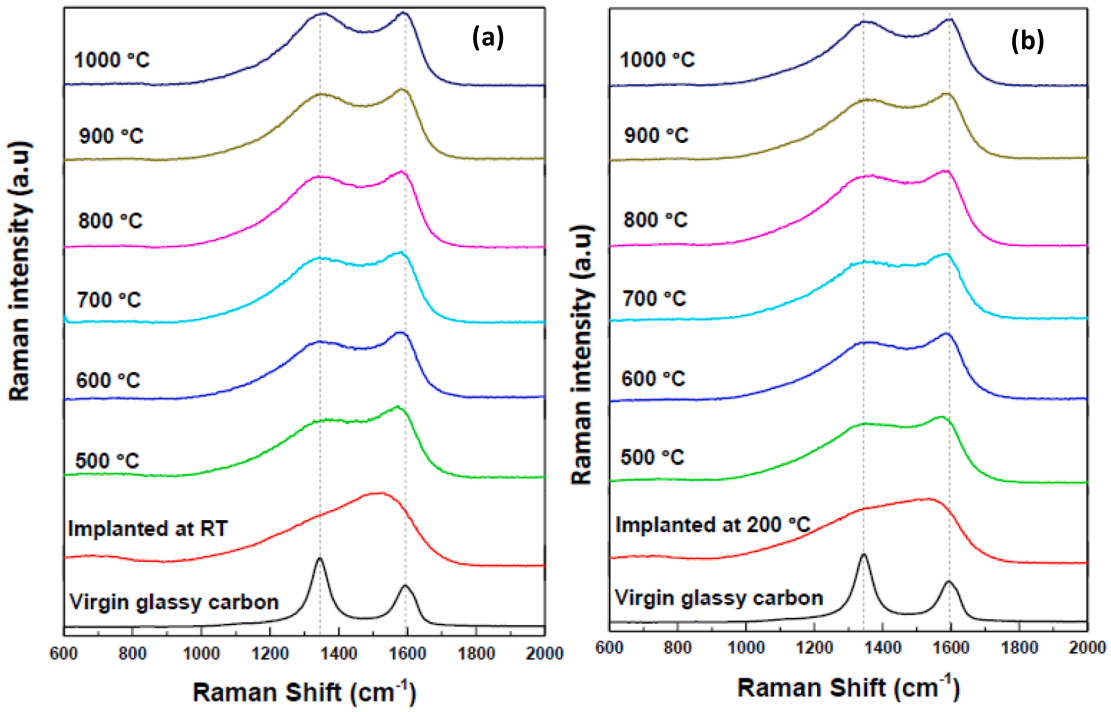

Fig. 3. Raman spectra of glassy carbon before and after ruthenium implantation at (a) room temperature and (b) 200 °C, and after annealing the implanted glassy carbon samples from 500– 1000 °C.

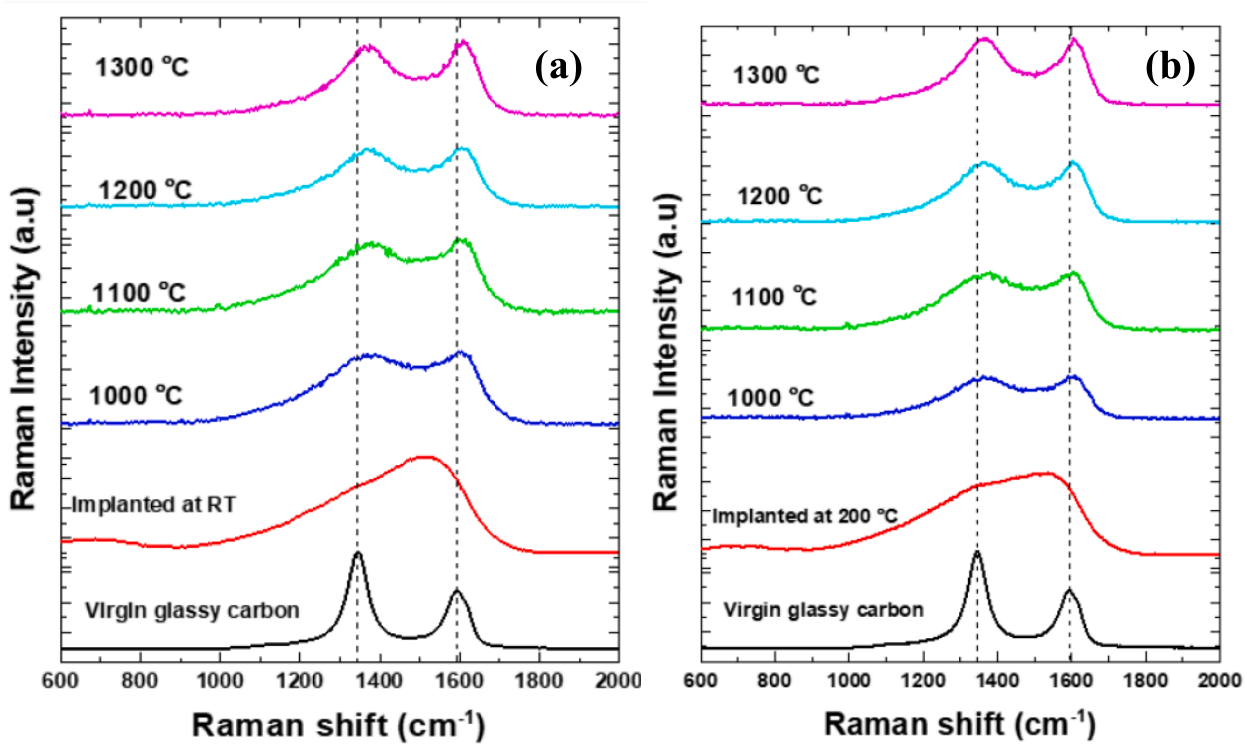

Fig. 4. Raman spectra of glassy carbon before and after ruthenium implantation at (a) room temperature and (b) 200 °C, and after annealing the implanted glassy carbon samples from 1000– 1300 °C.

implantation. Samples implanted at room temperature exhibit more shifts to a lower wavenumber than for samples implanted at 200 °C. Several factors influence residual stress in materials, including heat, implantation, and crystal growth. However, several studies by McCulloch *et al.* [25,30,33] found that an increase in the density of virgin glassy carbon after ion implantation at room temperature leads to the introduction of tensile stress in the glassy carbon. McCulloch *et al.* [25,30,33] mentioned that the increase in the density of the implanted glassy carbon will require a smaller volume (since density = mass/volume), then glassy carbon tends to contract, however, is prevented from

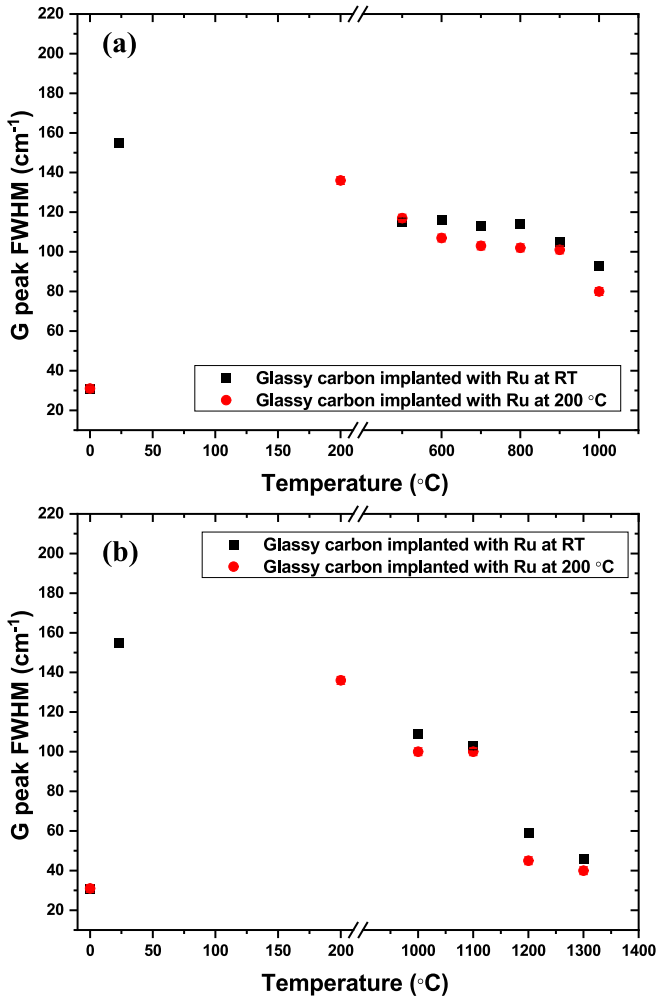

Fig. 5. FWHM values of the G peak of glassy carbon before and after ruthenium ion implantation at room temperature and 200 °C, and after annealing at (a) low (500 – 1000 °C) and (b) high (1000 – 1300 °C) temperatures. The FWHM of virgin glassy carbon are shown at 0 °C. Temperatures for implantation and annealing are separated by the break in the x-axis.

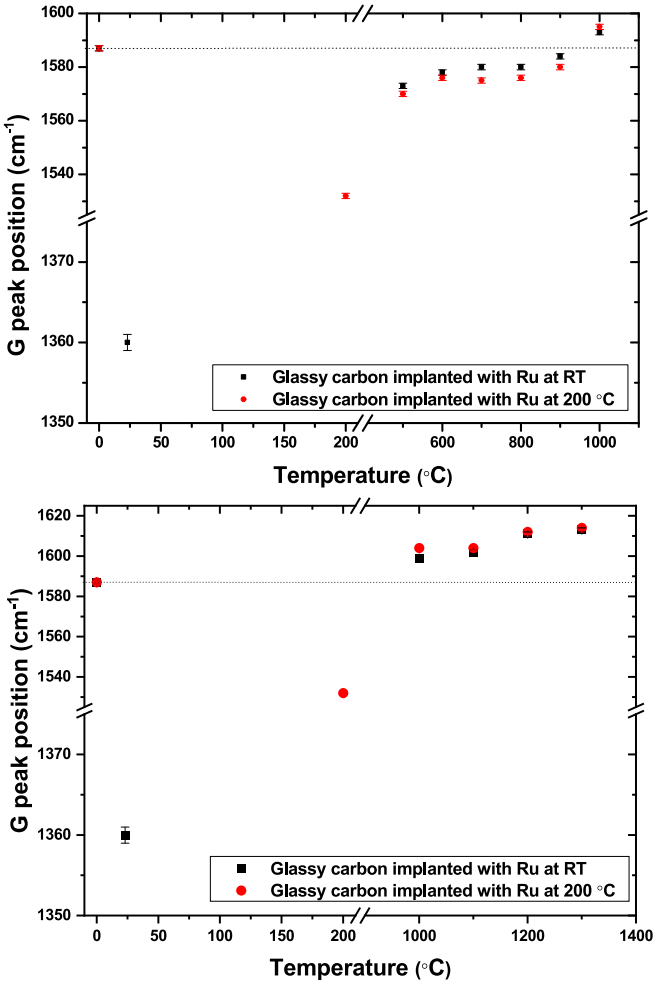

Fig. 6. The G peak position of the acquired spectra after Ru ions implantation and heat treatment at temperatures ranging from (a) 500 to 1000 °C and from (b) 1000 to 1300 °C. The position of the G peak of virgin GC is shown at 0 °C. Although error bars were included, their values are small to be clearly visible. Temperatures for implantation and annealing are separated by the break in the x-axis.

doing so in the plane of the substrate, giving rise to a tensile biaxial stress.

Annealing the as-implanted samples from 500 to 900 °C showed a significant shift of the G peak towards the higher wavenumber, but did not exceed the position of the G peak of virgin glassy carbon – see Fig. 6 (a). This indicates the reduction of tensile stress in glassy carbon after annealing up to 900 °C. However, annealing at 1000 °C or higher temperatures showed an increased shift of the G peak towards a wavenumber higher than the position of the G of virgin glassy carbon – see Fig. 6(a) and (b). The shift to higher wavenumber indicates the presence of the compressive stress [32]. An earlier study [34], found similar results, where Xe implantation into glassy carbon introduced tensile stress while sequential annealing from 500 to 900 °C reduced the tensile stress. However, they also found that sequential annealing up to 1000 °C induced compressive stress [34]. The difference in stress between as-implanted and annealed samples from 500 to 900 °C and from 1000 to 1300 °C could be due to differences in the glassy carbon density. McCulloch *et al.* [30] and Zhang *et al.* [35] found that annealing glassy carbon at temperatures around 1000 °C or higher reduces the density of glassy carbon due to structural rearrangement formation. Reducing the density of the implanted glassy carbon after annealing will result in compressive stress [33]. McCulloch *et al.* [33] mentioned that the decrease in the density will require a larger volume, thus glassy carbon will tend to expand, however, is prevented from doing so in the plane of the substrate, giving rise to a compressive biaxial stress. This agrees with the result presented in this study, where compressive stress was observed after annealing at temperatures above 900 °C.

3.3. XRD results

The amount and type of strain in virgin glassy carbon after implantation and annealing at high temperatures (from 1000 to 1300 °C) was estimated from XRD patterns (see Figures S1 and S2) using the William-Hall equation [36] – see Fig. 7. The amount of strain in virgin glassy carbon increased from 4.5×10^{-4} to 0.002 and 0.0054 after ion implantation at 200 °C and RT, respectively, indicating that ion implantation caused radiation damage (i.e., disorder within the graphitic crystallites in the glassy carbon structure) [37]. However, the strain in annealed samples has negative values – see Fig. 7. The minus sign or plus sign in the amount of strain indicates the type of strain: the minus sign indicates compressive strain, while the plus sign indicates tensile strain [38]. Therefore, as seen in Fig. 7, implantation of Ru in glassy carbon produced tensile strain, while annealing the as-implanted samples introduced compressive strain in the glassy carbon. This is in good agreement with Raman results, where the G peak position of virgin glassy carbon shifted to a lower wavenumber after implantation,

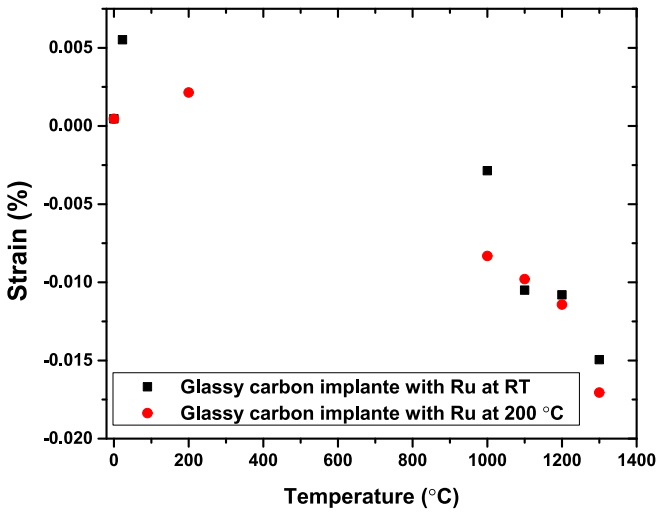

Fig. 7. Residual strain in virgin glassy carbon (at 0 °C) after implantation (at room temperature, i.e., 23 °C, and 200 °C) and annealing obtained from XRD data.

indicating the presence of the tensile strain. However, the G peaks shift to a higher wave number after annealing from 1000 to 1300 °C, which indicates the presence of compressive strain. As mentioned above, the difference in strain/stress between as-implanted and annealed samples could be due to differences in the glassy carbon density after implantation and annealing [25,30,33].

3.4. RBS results

Fig. 8 shows the depth profiles of Ru in glassy carbon before and after annealing at low temperatures (i.e., from 500 to 1000 °C). These depth profiles were fitted with an in-house program to obtain the projected range, R_p and the full width at half maximum FWHM [39], which is shown in Figs. 9 and 10, respectively. From Fig. 8, annealing from 500 to 800 °C showed no noticeable change in Ru depth profiles as compared to the as-implanted depth profile, which indicates the non-diffusivity of Ru in glassy carbon after annealing at these temperatures. However, annealing at 900 °C and 1000 °C caused a significant change in R_p and FWHM of ruthenium depth profiles as shown in Fig. 9. The R_p in room temperature implanted samples changed from 116 nm (for as-implanted samples) to 98 and 95 nm after annealing at 900 °C and 1000 °C, respectively, while the R_p in the 200 °C implanted samples changed to 96 nm and 93 nm, respectively – see Fig. 9 (a). This indicates that the depth profile has shifted toward the glassy carbon surface. The reason for this shift will be discussed later in this study – see discussion of Fig. 9 (a). Moreover, the shift was accompanied by a decrease in the FWHM from 0.66×10^{-14} m^2 (for as-implanted samples) to 0.60×10^{-14} m^2 and 0.58×10^{-14} m^2 for 200 °C implanted samples annealed at 900 °C and 1000 °C, respectively – see Fig. 9 (b). The room temperature implanted samples showed a greater decrease in FWHM, 0.46×10^{-14} m^2 and 0.40×10^{-14} m^2 after annealing at 900 °C and 1000 °C, respectively. Furthermore, the maximum peak of the relative atomic density in the room temperature implanted samples annealed at 900 °C and 1000 °C increased from around 1.8 % (for as-implanted samples) to 2.0 % and 2.2 %, respectively, while in the 200 °C implanted samples annealed under the same conditions was 1.9 % and 1.95 %, respectively.

These changes in the FWHMs and the maximum peaks of the relative atomic density indicate that the Ru atoms aggregate (i.e., high Ru concentration) in a smaller region (i.e., narrower FWHM) after annealing at 900 °C and 1000 °C as compared to the distribution of Ru atoms before and after annealing from 500 to 800 °C. Usually, the aggregation of atoms occurs due to cohesive forces between the atoms themselves, which leads to the formation of a cluster or particle [40]. Ru atoms have

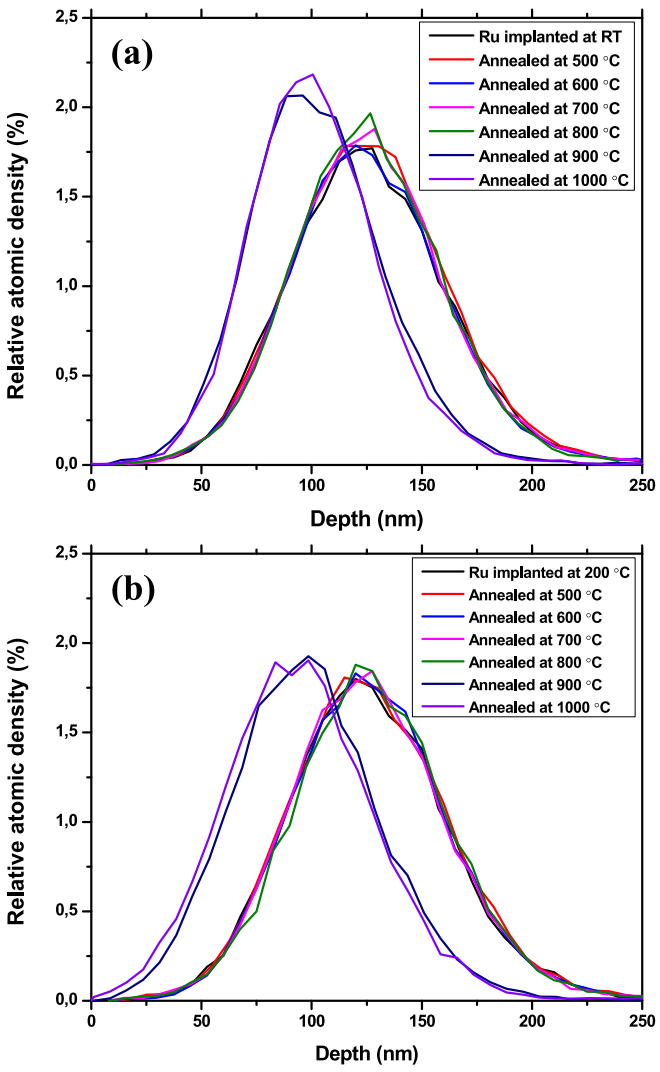

Fig. 8. RBS depth profiles of Ru implanted at (a) RT and (b) 200 °C, showing the effect of annealing at low temperature (500–1000 °C) on the migration behaviour.

strong cohesive forces (6.74 eV/atom) [41]; thus, the Ru atoms may easily tend to aggregate into "nanoparticles" in the glassy carbon. Several studies have shown that, during annealing, the metal atoms implanted into the substrate will aggregate to form metal nanoparticles inside the substrate [40,42–45]. Moreover, apart from these changes in the peaks positions, FWHM and the maximum of the relative atomic density peaks, no Ru concentration loss was observed after annealing.

From Fig. 8 (a) and (b), more Ru aggregation (higher relative atomic density and smaller FWHM) was observed in room temperature implanted samples compared to 200 °C implanted samples, all annealed at 900 °C and 1000 °C. This could be due to the higher concentration of defects in room temperature implanted samples (as discussed in Raman results), where defects in glassy carbon may lead to increased Ru aggregation and formation of clusters. It is consistent with the assumption that impurity clusters are more likely to form in regions with high defect concentrations (in the substrate) [46].

Moreover, Ru aggregation was accompanied by a peak shift toward the surface – see Fig. 9 (a). This behavior is not uncommon in other systems (e.g. see [47,48,49] for examples in SiC) and depends on changes in the surface microstructure (for example, thermal etching) of the substrate in which diffusion occurs. However, the shifting of the profiles towards the surface of glassy carbon is much more problematic to explain, as glassy carbon is thermally stable up to 2000 °C (i.e., with

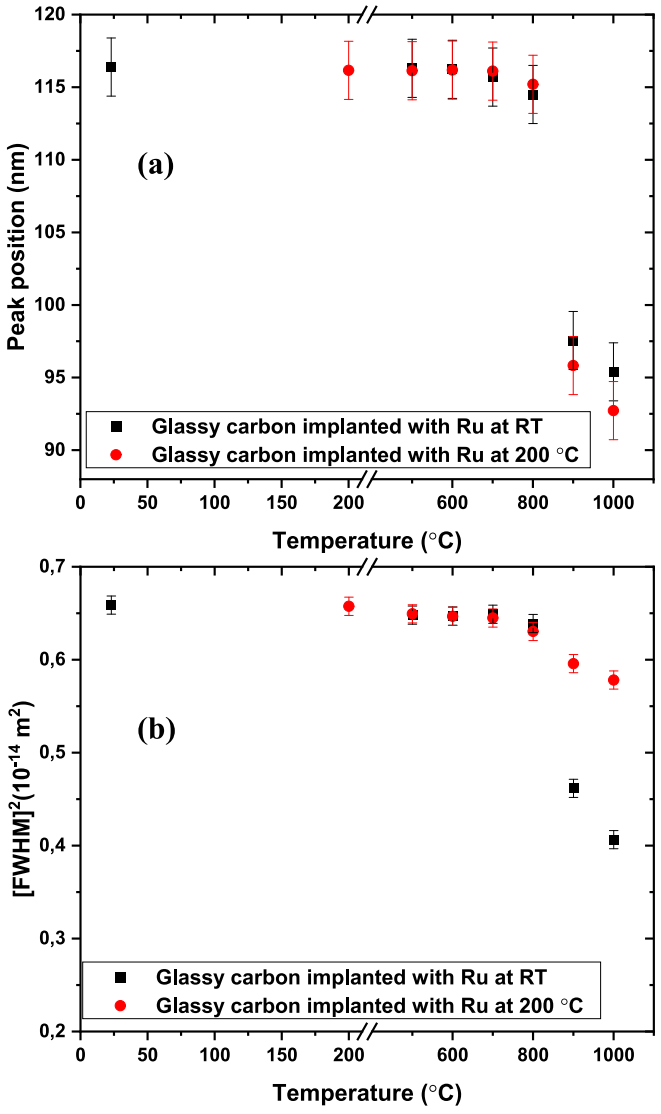

Fig. 9. (a)Peak positions of RBS Ru depth profiles (implanted at RT and 200 °C), then sequentially annealed from 500 °C to 1000 °C for 5 h. (b) FWHMs of RBS Ru depth profiles (implanted at RT and 200 °C), then sequentially annealed from 500 °C to 1000 °C for 5 h. Temperatures for implantation and annealing are separated by the break in the x-axis.

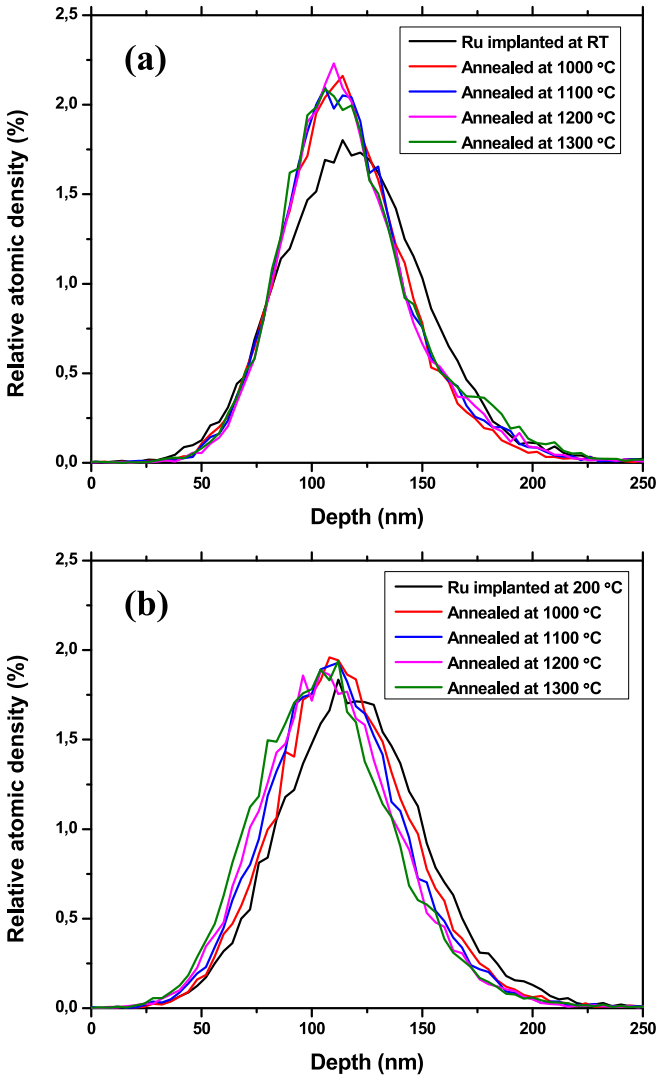

Fig. 10. Depth profiles of Ru implanted at (a) RT and (b) 200 °C, showing the effect of annealing at high temperature (1000–1300 °C) on the migration behavior of Ru.

no thermal etching) [50]. The peak shift toward the surface is probably due to a stress field leading to a migration of the profile as a whole [51]. The Raman and XRD results showed that Ru implantation and annealing introduced high levels of stress in the implanted region, which could cause Ru inclusions to drift towards the glassy carbon surface.

The RBS depth profiles of Ru in glassy carbon before and after annealing at high temperatures (1000 to 1300 °C) were compared as shown in Fig. 10. Furthermore, the changes in peak positions and FWHMs of the depth profiles due to annealing are shown in Fig. 11 (a) and (b), respectively. From Fig. 10, the maximum peak of the relative atomic density of the as-implanted samples was 1.8 %. This value increased after annealing at 1000 °C to 2.17 % and 1.97 % for room temperature and 200 °C implanted samples, respectively. Moreover, annealing at 1000 °C caused a decrease in the FWHM from 0.66×10^{-14} m^2 (for the as-implanted samples) to 0.35×10^{-14} m^2 and 0.47×10^{-14} m^2 for the samples implanted at room temperature and 200 °C, respectively. This indicates that annealing at 1000 °C caused Ru atoms to aggregate, as expected since Ru atoms tend to aggregate in glassy carbon at temperatures higher than 800 °C. However, comparing the FWHMs and the maximum peaks of the relative atomic density in the two samples, Ru aggregation was more pronounced in room temperature implanted samples than in 200 °C implanted samples, all annealed at 1000 °C. As discussed above, the high concentration of defects in room temperature implanted samples facilitated Ru aggregation and cluster formation. Moreover, as observed in samples annealed at lower temperatures, the shift in depth profile peak towards the glassy carbon surface could be due to a stress field. Subsequent annealing at 1100, 1200, and 1300 °C showed no significant Ru peak shift in room temperature implanted samples. Conversely, significant peak shifts were observed in 200 °C implanted samples after annealing under the same conditions (see Fig. 11 (a)). This might be due to increased Ru aggregation within the room temperature implanted samples (see Fig. 11(b)) which can cause Ru clusters to grow larger, causing Ru to migrate more slowly toward the surface compared to the 200 °C implanted samples which showed less Ru aggregation. Another explanation might be that the high concentration of defects in the room temperature implanted sample (compared to 200 °C implanted samples) can play a role in trapping the majority of the Ru atoms in the high radiation damage region which restricts its migration towards the surface. Similar results were found in a previous study [17], where Se atoms implanted in glassy carbon at room temperature showed less migration towards the surface

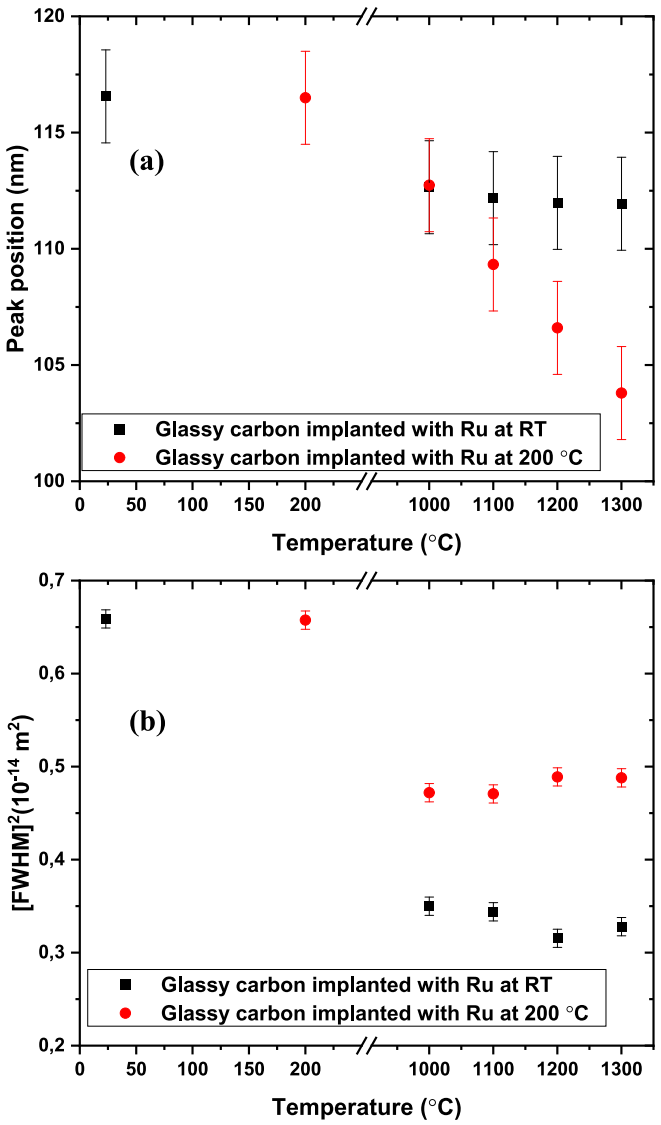

Fig. 11. (a) Peak positions of Ru depth profiles (implanted at RT and 200 °C), then sequentially annealed from 1000 °C to 1300 °C for 5 h. (b) FWHMs of Ru depth profiles (implanted at RT and 200 °C), then sequentially annealed from 1000 °C to 1300 °C for 5 h. Temperatures for implantation and annealing are separated by the break in the x-axis.

after annealing, compared to those implanted at 200 °C and annealed under the same conditions. This was explained by the higher radiation damage in room temperature implanted samples, which trapped the Se atoms [17]. Moreover, no noticeable loss of Ru implanted in glassy carbon was observed in the room temperature and 200 °C implanted samples, annealed between 1000 and 1300 °C. This can be attributed to Ru aggregation, which forms Ru clusters within the glassy carbon, thereby inhibiting Ru out-surface diffusion.

Comparing the FWHM of the RBS Ru depth profiles for samples annealed at 1000 °C (Fig. 11(b)) and sequentially up to 1000 °C (Fig. 9 (b)) is another key consideration. The narrower FWHM observed in the samples annealed at 1000 °C suggests higher levels of Ru aggregation in glassy carbon compared to those annealed sequentially up to 1000 °C. This difference could be due to partial removal of defects during sequential annealing from 500 to 900 °C, as indicated by the Raman results (see Fig. 5). Thus, defects in glassy carbon contribute significantly to Ru aggregation. Compared to sequentially annealed samples up to 1000 °C, glassy carbon samples annealed at 1000 °C exhibit greater aggregation and less Ru peak shift toward the surface (Figs. 9 and 11). Therefore, large Ru aggregation may inhibit the migration of Ru to the surface.

According to the above results, the migration of Ru in glassy carbon is affected by two factors – first, the concentration of defects in the as-implanted glassy carbon and second, the annealing temperature. Annealing from 500 to 800 °C caused no Ru migration in glassy carbon, however, higher temperatures (from 900 to 1300 °C) did. This indicates that Ru is non-diffusible in glassy carbon at temperatures below 900 °C. Moreover, Ru migration was highly affected by defects concentrations in glassy carbon as follows:

1. The high defect concentrations in the room temperature implanted samples trapped Ru atoms which aggregated and formed large clusters and thus hindered their migration toward the surface
2. On the other hand, the low defect concentrations in the 200 °C implanted samples caused less Ru trapping and thus reduced aggregation or formation of larger clusters. Therefore, Ru migration toward the surface was more pronounced in 200 °C implanted samples. This is due to the fact that less trapping caused lighter Ru aggregation or clusters which migrated easily toward the surface

3.5. AFM results

The surface roughness of virgin, as-implanted and annealed glassy carbon was evaluated by the AFM images (see Figures S3, S4, S5 and S6) and by measuring the R_q (root mean square roughness) using the Nanoscope software [22]. The R_q value obtained for virgin glassy carbon is 1.45 ± 0.1 nm. This value decreased to 0.40 ± 0.05 nm and 0.37 ± 0.05 nm after implantation of Ru at room temperature and 200 °C, respectively – see Fig. 12. In fact, the surface roughness of as-implanted glassy carbon at room temperature is no different from the surface roughness of samples implanted at 200 °C, which falls within measurement error. A reduction in surface roughness of virgin glassy carbon may be attributed to the Ru implantation. It is widely known that ion implantation often reduces the surface roughness of an initially rough surface [52]. On the other hand, depending on the substrate material, ion implantation can increase the surface roughness of an initially smooth surface [24,53,54]. In this study, the surface of the initial glassy carbon substrate was rough (i.e., 1.45 ± 0.1 nm), and decreased after implantation by Ru ions (as rough surfaces become smoother by

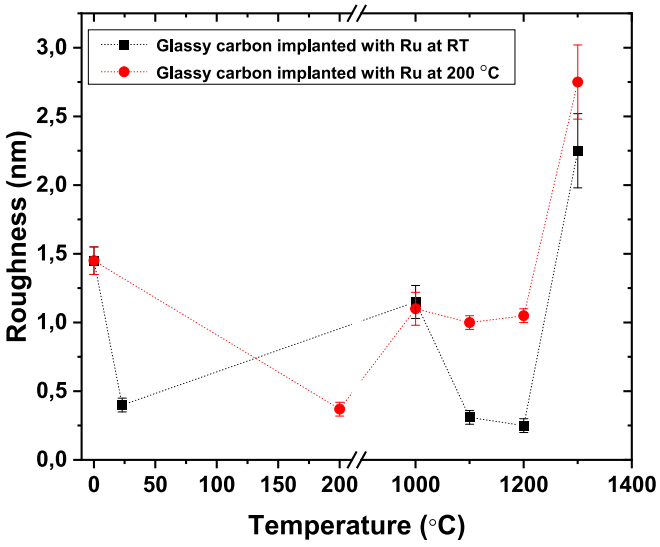

Fig. 12. Graph showing the effect of ruthenium implantation at room temperature (i.e., 23 °C) and 200 °C and annealing on the surface roughness of virgin glassy carbon (value at 0 °C) as determined by AFM. Temperatures for implantation and annealing are separated by the break in the x-axis.

sputtering [55]), indicating that Ru implantation reduced the surface roughness which is consistent with the above statement [52].

Fig. 12 shows the surface roughness values of glassy carbon after annealing at high temperatures. From Fig. 12, annealing at 1000 °C caused the surface roughness to increase significantly, reaching 1.10 ± 0.12 nm for the 200 °C implanted samples and 1.15 ± 0.12 nm for the room temperature implanted samples. The aggregation of ruthenium atoms at 1000 °C (see Fig. 10) may result in the formation of ruthenium nanoparticles near the surface, consequently increasing the surface roughness of glassy carbon. Similar findings were reported by Naidoo *et al.* [56], where increased surface roughness was observed in amorphous carbon upon Ag implantation, which was attributed to the formation of Ag nanoparticles in the near-surface region.

For room temperature implanted samples, annealing at 1100 and 1200 °C reduced surface roughness to 0.31 ± 0.05 nm and 0.25 ± 0.05 nm respectively. Since there is no further aggregation or migration of Ru after annealing the room temperature implanted glassy carbon samples at 1100 and 1200 °C (see Fig. 10 (a)), the effect of Ru migration on the surface roughness is negligible. However, annealing reduces the surface roughness (see Fig. 12) due to the surface diffusion of the substrate atoms (i.e., carbon atoms) at the peaks of the sputter roughened surface to valley positions. Consequently, polishing marks were less pronounced after annealing as shown in AFM images in Figure S5 (a) and (b). However, annealing the 200 °C implanted samples at 1100 and 1200 °C resulted in no change in surface roughness. This could be due to the further shift of the depth profile toward the surface at 1100 and 1200 °C (see Fig. 10 (b)) resulting in an increase in surface roughness. However, annealing at 1100 and 1200 °C reduces the surface roughness, competing with the increase in roughness caused by Ru migration, and leaving the surface roughness unchanged.

It was observed that annealing at 1300 °C resulted in an increase in the roughness values, which became 2.25 ± 0.27 nm for the room temperature implanted samples and 2.75 ± 0.27 nm for the 200 °C implanted samples. An increase in roughness could be due to the large island clusters formed on the surface of glassy carbon after annealing at 1300 °C. The results obtained from SEM images after annealing from 1000 °C to 1300 °C (as shown in Figures S7 and S8) confirmed these findings where the grains became larger and the surface became rougher at 1300 °C, compared to the samples annealed at 1000 °C. As the annealing temperature increased, the quantity of these clusters increased. This could be attributed to the aggregation of surface granules into large clusters at high temperatures. Surface morphology was observed to be affected by cluster size, namely, as cluster size and the number of clusters increased, the surface appeared rougher. The increase in cluster size was also accompanied by a reappearance of polishing marks, especially in the 200 °C implanted samples that exhibit higher roughness than the room temperature implanted samples annealed under the same conditions. This could be due to Ru migrating toward the surface in the 200 °C implanted samples annealed at 1300 °C, while no noticeable Ru migration was observed in the room temperature implanted samples – see Fig. 10. It can be deduced that the physical appearance of the surface topography is greatly dependent on heat treatment or the migration and aggregation of implanted Ru.

4. Summary and conclusion

This study investigated the structural changes in glassy carbon after ruthenium implantation (at room temperature and 200 °C) and annealing. Moreover, the migration behavior of ruthenium in glassy carbon was also studied. Raman spectroscopy showed that ruthenium implantation caused defects in the glassy carbon structures, with more defects observed in the room temperature as-implanted samples. These defects were reduced by annealing, however, samples implanted at room temperature still had a larger amount of defects compared to those implanted at 200 °C and annealed under the same conditions. Moreover, ion implantation introduced tensile stress into the glassy carbon structure, while annealing from 500 to 900 °C reduced this stress. Conversely, annealing at higher temperatures (from 1000 to 1300 °C) introduced compressive stress. These findings were confirmed by GIXRD results, consistent with Raman results. This difference in stress between as-implanted and annealed samples from 500 to 900 °C and from 1000 to 1300 °C was attributed to differences in glassy carbon density.

From the RBS results, annealing at temperatures from 500 to 800 °C did not significantly alter the Ru depth profiles, indicating that Ru does not diffuse in glassy carbon at these temperatures. However, annealing at higher temperatures caused notable changes in the Ru depth profiles, with increased aggregation of Ru atoms and a shift of the depth profiles toward the surface. This aggregation occurred due to strong cohesive forces between Ru atoms. Moreover, room temperature implanted samples exhibited more Ru aggregation than the 200 °C implanted samples. This is attributed to the higher concentration of defects in room temperature implanted samples, which facilitate Ru aggregation. The aggregation was accompanied by a shift of the whole depth profile towards the glassy carbon surface. This was probably due to a stress field that caused the profile to migrate as a whole. However, the shift of Ru depth profiles toward the surface was less pronounced in the room temperature implanted samples compared to 200 °C implanted samples, possibly due to the larger Ru clusters formed in these samples, hindering migration toward the surface. Moreover, remarkably, neither low-temperature nor high-temperature annealing led to significant loss of the implanted Ru from the glassy carbon.

From the AFM results, Ru implantation effectively reduces surface roughness in glassy carbon, with consistent results at different implantation temperatures. Annealing at 1000 °C leads to increased roughness due to Ru aggregation, while higher-temperature annealing has varying effects, influenced by factors such as surface diffusion, cluster formation and Ru migration.

CRediT authorship contribution statement

T.A.O. Jafer: Writing – original draft, Methodology, Investigation, Formal analysis, Conceptualization. **O.S. Odutemowo:** Writing – review & editing. **H.A.A. Abdelbagi:** Writing – review & editing, Investigation. **T.T. Thabethe:** Writing – review & editing, Supervision. **J.B. Malherbe:** Writing – review & editing, Supervision, Resources.

Declaration of competing interest

The authors declare that they have no known competing financial interests or personal relationships that could have appeared to influence the work reported in this paper.

Data availability

Data will be made available on request.

Acknowledgements

Financial support from the Organization for Women in Science for the Developing World (OWSD) and the International Atomic Energy Agency (IAEA- contract number 28267) is gratefully acknowledged. The authors would like to thank Dr T. Ntsoane from NECSA for his assistance with XRD data collection.

Appendix A. Supplementary data

Supplementary data to this article can be found online at https://doi.org/10.1016/j.nimb.2024.165533.

References

[1] K. Saidi, A. Omri, Reducing CO_2 emissions in OECD countries: Do renewable and nuclear energy matter? Prog. Nucl. Energy 126 (2020) 103425.
[2] B. Merk, D. Litskevich, K.R. Whittle, M. Bankhead, R.J. Taylor, D. Mathers, On a long term strategy for the success of nuclear power, Energies 10 (2017) 867.
[3] J.B. Malherbe, O.S. Odutemowo, E.G. Njoroge, D.F. Langa, T.T. Hlatshwayo, C. C. Theron, Ion bombardment of glassy carbon, Vacuum 149 (2018) 19–22.
[4] M.V. Ramana, Technical and social problems of nuclear waste, Wiley Interdiscipl. Rev. Energy Environ. 7 (2018) 289.
[5] R.M. Carranza, M.A. Rodríguez, Crevice corrosion of nickel-based alloys considered as engineering barriers of geological repositories, npj Mater. Degrad. 1 (2017) 1–9.
[6] A.J. Innocent, T.T. Hlatshwayo, E.G. Njoroge, T.P. Ntsoane, M. Madhuku, E. O. Ejeh, M. Mlambo, M.Y.A. Ismail, C.C. Theron, J.B. Malherbe, Evaluation of diffusion parameters and phase formation between tungsten films and glassy carbon, Vacuum 175 (2020) 109245.
[7] S.A. Adeojo, J.B. Malherbe, E.G. Njoroge, M. Mlambo, O.S. Odutemowo, T. T. Thabethe, Z.A.Y. Abdalla, T.T. Hlatshwayo, Effect of sequential isochronal annealing on the structure and migration behaviour of selenium-ion implanted in glassy carbon, Vacuum 182 (2020) 109689.
[8] M.Y.A. Ismail, J.B. Malherbe, O.S. Odutemowo, E.G. Njoroge, T.T. Hlatshwayo, M. Mlambo, E. Wendler, Investigating the effect of heat treatment on the diffusion behaviour of xenon implanted in glassy carbon, Vacuum 149 (2018) 74–78.
[9] T.T. Hlatshwayo, L.D. Sebitla, E.G. Njoroge, M. Mlambo, J.B. Malherbe, Annealing effects on the migration of ion-implanted cadmium in glassy carbon, Nucl. Instrum. Methods Phys. Res. B. 395 (2017) 34–38.
[10] E.G. Njoroge, T.T. Hlatshwayo, M. Mlambo, O. Odutemowo, K.A. Annan, A. Skuratov, M. Ismail, J.B. Malherbe, Effect of thermal annealing on SHI irradiated indium implanted glassy carbon, Nucl. Instrum. Methods Phys. Res. B. 502 (2021) 66–72.
[11] E.G. Njoroge, L.D. Sebitla, C.C. Theron, M. Mlambo, T.T. Hlatshwayo, O. S. Odutemowo, V.A. Skuratov, E. Wendler, J.B. Malherbe, Structural modification of indium implanted glassy carbon by thermal annealing and SHI irradiation, Vacuum 144 (2017) 63–71.
[12] O.S. Odutemowo, M.S. Dhlamini, E. Wendler, D.F. Langa, M.Y.A. Ismail, J. B. Malherbe, Effect of heat treatment on the migration behaviour of Sr and Ag CO-implanted in glassy carbon, Vacuum 171 (2020) 109027.
[13] O.S. Odutemowo, J.B. Malherbe, L. Prinsloo, D.F. Langa, E. Wendler, High temperature annealing studies of strontium ion implanted glassy carbon, Nucl. Instrum. Methods Phys. Res. B. 371 (2016) 332–335.
[14] D.F. Langa, N.G. Van Der Berg, E. Friedland, J.B. Malherbe, A.J. Botha, P. Chakraborty, E. Wendler, W. Wesch, Heat treatment of glassy carbon implanted with cesium at room and high temperatures, Nucl. Instrum. Methods Phys. Res. B. 273 (2012) 68–71.
[15] O.S. Odutemowo, J.B. Malherbe, C.C. Theron, E.G. Njoroge, E. Wendler, In-situ RBS studies of strontium implanted glassy carbon, Vacuum 126 (2016) 101–105.
[16] M.Y.A. Ismail, Z.A.Y. Abdalla, E.G. Njoroge, O.S. Odutemowo, T.T. Hlatshwayo, E. Wendler, V.A. Skuratov, J.B. Malherbe, Effect of high temperature annealing and SHI irradiation on the migration behaviour of Xe implanted into glassy carbon, Nucl. Instrum. Methods Phys. Res. B. 489 (2021) 11–19.
[17] S. Adeojo, J. Malherbe, A. Azarov, O. Odutemowo, E. Njoroge, H. Abdelbagi, S. Mpelane, T. Hlatshwayo, Effects of implantation temperature and annealing on structural evolution and migration of Se into glassy carbon, Solid State Sci. 129 (2022) 106914.
[18] T.A.O. Jafer, T.T. Thabethe, O.S. Odutemowo, S.A. Adeojo, H.A.A. Abdelbagi, A. Azarov, J.B. Malherbe, Ruthenium ion modification of glassy carbon: implication on the structural evolution and migration behaviour of implanted Ru atoms, Nucl. Instrum. Methods Phys. Res. B. 534 (2023) 72–80.
[19] Z. Ni, Y. Wang, T. Yu, Z. Shen, Raman spectroscopy and imaging of graphene, Nano Res. 1 (2008) 273–291.
[20] K.J. Stevenson, Review of originpro 8.5, J. Am. Chem. Soc. 133 (2011) 5621.
[21] AFM Resource Library-Agilnet Technology. Available online: http://www.afmuniversity.org (accessed on 28 April 2024).
[22] NanoScope Software 6.13 User Guide, V.I.I. Version; Veeco Instruments Inc.: Plainview, NY, USA, 2004.
[23] J. Ziegler, *SRIM 2012 computer code*, 2012. URL: www.srim.org.
[24] O.S. Odutemowo, J.B. Malherbe, L.C. Prinsloo, E.G. Njoroge, R. Erasmus, E. Wendler, A. Undisz, M. Rettenmayr, Structural and surface changes in glassy carbon due to strontium implantation and heat treatment, J. Nucl. Mater. 498 (2018) 103–116.
[25] D. McCulloch, S. Prawer, A. Hoffman, Structural investigation of xenon-ion-beam-irradiated glassy carbon, Phys. Rev. B 50 (1994) 5905.
[26] A. Orlando, F. Franceschini, C. Muscas, S. Pidkova, M. Bartoli, M. Rovere, A. Tagliaferro, A comprehensive review on Raman spectroscopy applications, Chemosensors 9 (2021) 262.
[27] S.R.P. Silva, Properties of amorphous carbon, INSPEC, London, UK, 2003.
[28] A.C. Ferrari, J. Robertson, Interpretation of Raman spectra of disordered and amorphous carbon, Phys. Rev. B 61 (2000) 14095–14107.
[29] M. Yoshikawa, G. Katagiri, H. Ishida, A. Ishitani, T. Akamatsu, Raman spectra of diamond-like amorphous carbon films, J. Appl. Phys. 64 (1988) 6464–6468.
[30] D.G. McCulloch, S. Prawer, The effect of annealing and implantation temperature on the structure of C ion beam irradiated glassy carbon, J. Appl. Phys. 78 (1995) 3040–3047.
[31] K. Niwase, Irradiation-induced amorphization of graphite, Phys. Rev. B 52 (1995) 15785–15798.
[32] E. Wendler, T. Bierschenk, F. Felgentrager, J. Sommerfeld, W. Wesch, D. Alber, G. Bukalis, L.C. Prinsloo, N. van der Berg, E. Friedland, J.B. Malherbe, Damage formation and optical absorption in neutron irradiated SiC, Nucl. Instrum. Methods Phys. Res. B. 286 (2012) 97–101.
[33] D.G. McCulloch, R. Mc Kenzie, S. Prawer, Compressive stress induced formation of preferred orientation in glassy carbon following high-dose C^+ implantation, Philos. Mag. A 72 (4) (1995) 1031–1041.
[34] M.Y.A. Ismail, The Migration Behaviour Of Xenon Implanted Into Glassy Carbon, University of Pretoria, 2019. Diss.
[35] Z.I. Zhang, R. Brydson, Z. Aslam, S. Reddy, A. Brown, A. Westwood, B. Rand, Investigating the structure of non-graphitising carbons using electron energy loss spectroscopy in the transmission electron microscope, Carbon 49 (2011) 5049–5063.
[36] G.K. Williamson, W.H. Hall, X-ray line broadening from filed aluminium and wolfram, Acta Metall. 1 (1953) 22–31.
[37] R.A. Khmelnitsky, V.A. Dravin, A.A. Tal, M.I. Latushko, A.A. Khomich, A. V. Khomich, A.S. Trushina, A.A. Alekseev, S.A. Terentiev, Mechanical stresses and amorphization of ion-implanted diamond, Nucl. Instrum. Meth. Phys. Res. B 304 (2013) 5–10.
[38] G.C.A.M. Janssen, Stress and strain in polycrystalline thin films, stress and strain in polycrystalline thin films, Thin Solid Films. 515 (2007) 6654–6664.
[39] J.B. Malherbe, P.A. Selyshchev, O.S. Odutemowo, C.C. Theron, E.G. Njoroge, D. F. Langa, T.T. Hlatshwayo, Diffusion of a mono-energetic implanted species with a Gaussian profile, Nucl. Instrum. Meth. Phys. Res. B 406 (2017) 708–713.
[40] J.E. Lennard-Jones, The migration and aggregation of atoms on solid surfaces, Proc. Phys. Soc. (1926-1948) 49 (4S) (1937) 140.
[41] E. Kaxiras, Atomic and Electronic Structure of Solids, Cambridge University Press, Cambridge, 2003.
[42] G.W. Arnold, J.A. Borders, Aggregation and migration of ion-implanted silver in lithia-alumina-silica Glass, J. Appl. Phys. 48 (1977) 1488–1496.
[43] R.A. Wood, P.D. Townsend, N.D. Skelland, D.E. Hole, J. Barton, C.N. Afonso, Annealing of ion implanted silver colloids in glass, J. Appl. Phys. 74 (1993) 5754–5756.
[44] A. Miotello, G.D. Marchi, G. Mattei, P. Mazzoldi, C. Sada, Clustering of gold atoms in ion-implanted silica after thermal annealing in different atmospheres, Phys. Rev. B 63 (2001) 075409.
[45] V. Resta, G. Quarta, L. Maruccio, L. Calcagnile, Copper ion implantation of polycarbonate matrices: Morphological and structural properties, Nucl. Instrum. Meth. Phys. Res. B 331 (2014) 187–190.
[46] V.N. Kozyrenko, I.D. Mikhailov, The effect of the impurity cluster on the vibrational spectrum of a one-dimensional crystal, Phys. Status Solidi (B) 59 (1973) 13–16.
[47] J.B. Malherbe, Diffusion of fission products and radiation damage in SiC, J. Phys. D Appl. Phys. 46 (2013) 473001.
[48] H.A.A. Abdelbagi, V.A. Skuratov, S.V. Motloung, E.G. Njoroge, M. Mlambo, J. B. Malherbe, J.H. O'Connell, T.T. Hlatshwayo, Effect of swift heavy ions irradiation in the migration of silver implanted into polycrystalline SiC, Nucl. Instrum. Methods Phys. Res. B 461 (2019) 201–209.
[49] H.A.A. Abdelbagi, V.A. Skuratov, S.V. Motloung, E.G. Njoroge, M. Mlambo, T. T. Hlatshwayo, J.B. Malherbe, Effect of swift heavy ions irradiation on the migration behavior of strontium implanted into polycrystalline SiC, Nucl. Instrum. Methods Phys. Res. B 451 (2019) 113–121.
[50] V. Uskokovic, A historical review of glassy carbon: Synthesis, structure, properties and applications, Carbon Trends 5 (2021) 100116.
[51] S. Nsengiyumva, A.T. Raji, J.P. Riviere, D.T. Britton, M. Harting, Stress enhanced diffusion of krypton ions in polycrystalline titanium, J. Appl. Phys. 116 (2014) 023513.
[52] M.A. Makeev, R. Cuerno, A.L. Barabasi, Morphology of ion sputtered surfaces, Nucl. Instr. and Meth. Phys. Res. B 197 (3–4) (2002) 185–227.
[53] Y.Y. Chang, Y.N. Shieh, H.Y. Kao, Optical properties of TiO_2 thin films after Ag ion implantation, Thin Solid Films 519 (2011) 6935–6939.
[54] A.L. Barabasi, H.E. Stanley (Eds.), Fractal Concepts in Surface Growth, Cambridge University Press, 1995.
[55] M. Wagner, M. Mayer, U. von Toussaint, A. Mutzke, Simulation of the evolution of rough surfaces by sputtering using the binary collision approximation, Radiat Eff. Defects Solids 177 (2022) 1019–1032.
[56] S.R. Naidoo, A. Ismaila, Fluence enhanced optical response of Ag implanted amorphous carbon thin films, C. 5 (2019) 45.